J Nanopart Res (2023) 25:209
https://doi.org/10.1007/s11051-023-05855-7

RESEARCH PAPER

PH_3 gas adsorption on S and Mo vacancy MoS_2 monolayer: a first principle study

Meribah Jasmine Jayachandran · Preferencial Kala C · John Thiruvadigal D

Received: 16 May 2023 / Accepted: 27 September 2023 / Published online: 11 October 2023

Abstract The sensing nature and change in the electron transport behavior of S vacancy armchair MoS_2 (AmS-MoS_2), Mo vacancy armchair MoS_2 monolayer (AmMo-MoS_2), S vacancy zigzag MoS_2 (ZigS-MoS_2), and zigzag Mo vacancy MoS_2 (ZigMo-MoS_2) monolayer before and after PH_3 adsorption were theoretically investigated using Density Functional Theory (DFT) in combination with Non-Equilibrium Greens Function (NEGF) based on first principle calculations. To study the feasibility of armchair and zigzag MoS_2 device as PH_3 gas sensor, we conducted an analysis of the changes in the geometrical structures, density of states (DOS), transmission spectrum, and I–V characteristic. Our results predicted that PH_3 adsorption on all four devices is through van der Waals interactions. Among the four devices, AmMo-MoS_2 shows enhanced adsorption behavior with the adsorption energy − 1.8048 eV and charge transfer of − 0.2120e. The I–V characteristic of AmMo-MoS_2 shows a significant change in the conductivity compared with the other devices. Thus, our work concluded that AmMo-MoS_2 is considered to be a better device for PH_3 adsorption compared with the other devices.

M. J. Jayachandran · P. Kala C (✉) · J. Thiruvadigal D
Centre for Materials Science and Nanodevices,
Department of Physics and Nanotechnology, SRM Institute of Science and Technology, Kattankulathur 603203, Tamil Nadu, India
e-mail: preferec@srmist.edu.in

Keywords Density Functional Theory (DFT) · Non-Equilibrium Greens Function (NEGF) · Phosphene (PH_3) · Van der Waals interactions · Electron transport study · Molybdenum disulfide (MoS_2) · Adsorption · Sensor

Introduction

Phosphine (PH_3) is a highly poisonous gas that is commonly used in semiconductor industries and for fumigating grains. PH_3 gas molecules are exhausted during the production of acetylene and flame-retardant industries. The emission of PH_3 gas is very harmful to human beings, which causes cancer, headache, vomiting, fatigue, and even cause damage to the heart [1–4]. Therefore, rapid and precise sensing and monitoring of PH_3 gas molecules play an essential role in prevention.

Two-dimensional materials (2D) have a tremendous attractive interest due to their unique and extraordinary mechanical, physical, and chemical properties [5]. It has been considered as a suitable material for various potential applications. It is also considered as flexible material for next-generation optoelectronic devices, electronic devices, and gas sensors [6–8]. For the past few years, the researchers found that graphene has earned much more attention for its unique properties, and it has been used in many applications. However, the absence of bandgap in graphene has limited their progress [6, 9]. Transition metal dichalcogenides (TMDs) are thin semiconductors of type MX_2 [10], where *M* is the transition metal element from groups IV, V, or VI and X represents the chalcogen elements like S, Se, and Te [11]. 2D materials have some attractive and interesting features, including high carrier mobility, high surface to volume ratio, high chemical stability, high thermal stability, low electronic temperature noise and fast response time [12, 13], and low-cost effect [14]. Materials with these characteristics are considered to be ideal for sensing applications [11, 15]. Among TMDs, MoS_2 (molybdenum disulfide) is considered one of the most suitable materials for electronic device and sensor applications due to its excellent electrical and mechanical properties [14] and tunable bandgap when compared with graphene [12, 16]. The crystal structure of MoS_2 consists of a weakly coupled S-Mo-S sandwich layer. The structure of MoS_2 monolayer can be fabricated by the micromechanical cleavage or exfoliation method [9, 17, 18].

Shokri and Salami analyzed the sensing capabilities of MoS_2 monolayer transducer with CO, CO_2 and NO gas molecules and concluded that the NO gas molecule shows more changes in the electronic properties and charge transfer while compared with CO, CO_2 gas molecules [19]. Jasmine et al. theoretically analyzed the sensing behavior of Cl_2, PH_3, AsH_3, BBr_3, and SF_4 gas molecules on Mo/S vacancy MoS_2 monolayer and concluded that the PH_3 gas molecule shows more adsorption towards S/Mo vacancy MoS_2 monolayer [10]. Ren et al. theoretically investigated the adsorption behavior of CH_3 gas molecule on S and Mo vacancy MoS_2 monolayer, and they suggested that the different vacancies have a different effect on adsorption behavior [20]. Feng et al. concluded that the material's conductivity is increased due to the vacancy creation [21]. Zhao et al. theoretically investigated the adsorption of various gas molecules, including CO, CO_2, NH_3, NO, NO_2, CH_4, H_2O, N_2, O_2, and SO_2 on MoS_2 monolayer using DFT. The results indicate that NO and NO_2 show better adsorption than other gas molecules [22]. Wei et al. theoretically investigated the sensing behavior of Ni-doped MoS_2 monolayer towards SO_2, H_2S, and SF_6 gas molecules. The results indicate that H_2S and SO_2 tend to adsorb on the surface of Ni-MoS_2 monolayer by chemisorption, and the adsorption energy of the H_2S and SO_2 are − 1.319 eV and − 1.382 eV, respectively [23]. Kumar et al. experimentally analyzed the recent progress and remarkable development in gas sensing field by using the 2D MoS_2. They have developed various fabrication techniques for synthesizing a wide range of different nanostructures and morphologies of the MoS_2 on rigid as well as flexible substrates. They concluded that all the exciting gas sensing results of the 2D MoS_2 could be the best candidate for developing a high-performance room temperature gas sensor [24]. Chacko et al. analyzed the experimental study of Ni and Pd functionalized MoS_2 devices towards H_2S and NO. The MoS_2-based sensors showed excellent sensing performances with high sensitivity at room temperature, which can serve as an excellent alternative to the standard semiconductor metal oxide gas sensors that require high optimal working temperatures for good response [25].

The main novelty of this work is to analyze the sensing nature, adsorption behavior, and the changes in the electron transport properties of S and Mo vacancy created MoS_2 towards PH_3 gas molecule. In recent works, researchers have been using MoS_2 for gas sensing applications. But we have analyzed the sensing nature of S and Mo vacancy created MoS_2 towards PH_3 gas molecule. Moreover, we have also constructed the armchair and zigzag device with two electrodes model and analyzed the changes in the electron transport properties using DFT combined with Non-Equilibrium Green's Function (NEGF) for PH_3 gas adsorption.

Computational details

A modeled structure of the MoS_2 device with S and Mo vacancy is represented in Fig. 1. We have constructed the MoS_2 device with 50 Mo atoms and 100 S atoms. The device consists of three parts, i.e., the left and right electrodes and central scattering region. The size of the central region is 19.55 Å (the central region is long enough to study the adsorption behavior of the gas molecule), and the size of the electrode is 3.16 Å which is chosen in such a way to study the effect of adsorption between the MoS_2 monolayer and the PH_3 gas molecule.

The electron transport properties for adsorption effects of PH_3 gas molecule on S and Mo vacancy MoS_2 monolayer are performed using DFT combined with NEGF [26]. The empirical correction DFT + D2 has been used to correct the effect of van der Waals

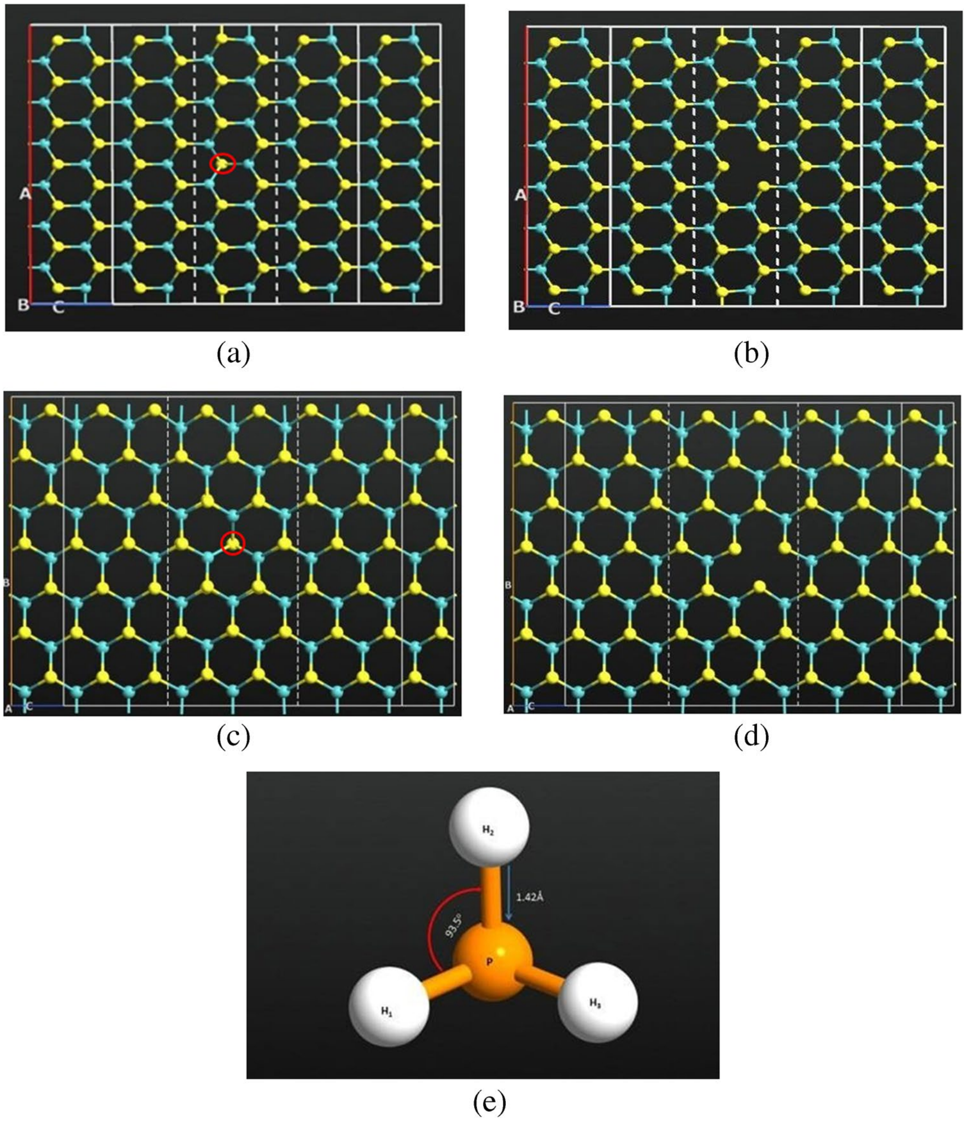

Fig. 1 Optimized structure of **a** AmS-MoS_2 device, **b** AmMo-MoS_2 device, **c** ZigS-MoS_2 device, and **d** ZigMo-MoS_2 device and **e** PH_3 gas molecule

interaction [27]. We utilized the virtual NanoLab simulation tool for constructing the MoS_2 device and the QuantumWise Atomistix Toolkit (ATK) package for performing the DFT calculations [27, 28].

The optimized geometry of Am-MoS_2 and Zig-MoS_2 with S and Mo vacancy is represented in Fig. 1. For optimization, we have used Linear Combination of Atomic Orbitals (LCAO) as basic set and Double Zeta plus polarization to solve the Kohn–Sham equations. For the geometrical optimization, we have used generalized gradient approximation (GGA) as an exchange–correlation function with Perdew–Burke–Ernzerhof (PBE) functional [19]. For energy tolerance, we have set the convergence criteria of 1.0×10^{-5} and the maximum force of 0.002 Ha/Å and 0.005 Å for the displacement of geometrical optimization. For accuracy calculation, the cutoff ratio has been set as 5.0 Å in the real space grid [27]. Zone integration is sampled with $2 \times 1 \times 100$ grid mesh along *x*-, *y*-, and *z*-directions, where the electron transport is along the *z*-direction. For relaxation calculation, the lattice parameters were set as

$a = b = 12.66$ Å and $c = 20.00$ Å [10, 27]. The atomic positions of all the geometries were fully optimized until the force on each atom becomes less than 0.05 eV/Å [10, 27, 29]. The temperature of the electron is taken as 300 K throughout the calculations [29–31]. The transmission spectrum was calculated using the transmission function at a particular bias. The transmission function $T(E,V)$ is given:

$$T(E, V) = Tr\left[\Gamma_L(E, V)G^R(E)\Gamma_R(E, V)G^A(E)\right] \quad (1)$$

Here, Γ_L and Γ_R represent the contact broadening functions of the left and right electrodes respectively. G^R and G^A represent the retarded advance Green's function. The current $I(V)$ can be calculated using $T(E,V)$, and it can be written as follows:

$$I(V) = \frac{2e^2}{h}\int_{\mu_L}^{\mu_R}\left[f\left(E-\mu_L\right)-f\left(E-\mu_R\right)\right]T(E,V)dE \quad (2)$$

where e, h, f, and E represented the electron charge, Plank's constant, Fermi function, energy respectively. μ_L and μ_R are the chemical potentials of the left and right electrodes.

The adsorption energy between the PH_3 gas molecule and armchair and zigzag MoS_2 monolayer with S and Mo vacancy is defined as follows:

$$E_{ads} = E_{PH_3V_{S/MO}MoS_2} - \left(E_{V_{S/MO}MoS_2} + E_{PH_3}\right) \quad (3)$$

where $E_{PH_3V_{S/MO}MoS_2}$ represents the total energy of S/Mo vacancy MoS_2 device after PH_3 adsorption on. $E_{V_{S/MO}MoS_2}$ represents the total energy of S/Mo vacancy created MoS_2 device. E_{PH_3} represents the total energy of the gas molecule. We have used Mulliken population analysis for charge transfer (Q) calculation. The difference between the actual valence of S/Mo atom and the valency charge obtained from Mulliken population analysis gives the charge of each and every individual atom in V_S and V_{Mo} MoS_2 monolayer. The net charge transfer of the system is calculated by the summation of all the differences obtained from Mulliken population analysis. From the net total, the negative sign indicated the charge transfer from V_S/V_{Mo} MoS_2 monolayer to PH_3 gas molecule and the positive value indicated the charge transfer from the PH_3 gas molecule to the V_S/V_{Mo} MoS_2 monolayer [10, 29] which are represented in Table 1. To get a deeper understanding of the electronic and

Table 1 The values of adsorption distance (d), adsorption energy (E_{ads}), charge transfer (Q), and changes in the bond length and bond angle

MoS_2 model	S/Mo vacancy	Adsorption distance d(Å)	Bond length (Å)			Bond angle (deg)			Adsorption energy E_{ads} (eV)	Charge transfer Q(e)
			(H_1P)	(H_2P)	(H_3P)	(H_1PH_2)	(H_2PH_3)	(H_3PH_1)		
PH_3 before adsorption	–	–	1.4200	1.4200	1.4200	93.50°	93.50°	93.5°	–	–
Armchair	S	2.6837	1.4262	1.3973	1.4404	96.72°	97.78°	96.17°	−0.9006	−0.0710
	Mo	2.3420	1.4428	1.4439	1.4433	98.17°	98.19°	98.32°	−1.8048	−0.2120
Zigzag	S	2.5204	1.4461	1.4429	1.4431	96.38°	96.04°	96.12°	−0.1234	−0.0720
	Mo	2.3627	1.4503	1.5142	1.4532	93.23°	114.30°	85.59°	−0.3522	−0.1800

sensing property, the changes caused in the charges after the adsorption of gas molecule are analyzed. In Fig. 1, the bond length between Mo atom and S atom is 2.415 Å, and between two S is 3.131 Å.

Results and discussion

To understand the adsorption effects of PH_3 gas molecule towards MoS_2 device, different adsorption configurations are calculated. The results include DOS, transmission spectrum, I-V curve, adsorption energy, and charge transfer.

Figure 2a–d shows the optimized structure of PH_3 adsorption on armchair S vacancy MoS_2 monolayer (AmS-MoS_2PH_3), PH_3 adsorption on armchair Mo vacancy MoS_2 monolayer (AmMo-MoS_2PH_3), PH_3 adsorption on zigzag S vacancy MoS_2 monolayer (ZigS-MoS_2PH_3), and PH_3 adsorption on zigzag Mo vacancy MoS_2 monolayer (ZigMo-MoS_2PH_3), respectively. In order to get a more stable configuration, the optimized PH_3 gas molecule is placed vertically above the vacancy created on the MoS_2 monolayer. From Fig. 2, we observed that there is a non-bonding interaction between the device and the gas molecule. This shows that the adsorption is through physisorption [32, 33]. After the adsorption, the structure of the PH_3 gas molecule dislocates, where the bond length P–H and bond angle HPH have been increased and decreased, and the changes are listed in Table 1. The changes in the bond length and bond angles are caused due to the van der Waals interaction [33]. From Table 1, we observed that the PH_3 adsorption on AmMo-MoS_2 and ZigMo-MoS_2 shows more change in the bond length and bond angle. For AmMo-MoS_2PH_3, the changes in the bond length are 1.4428 Å, 1.4439 Å, and 1.4433 Å

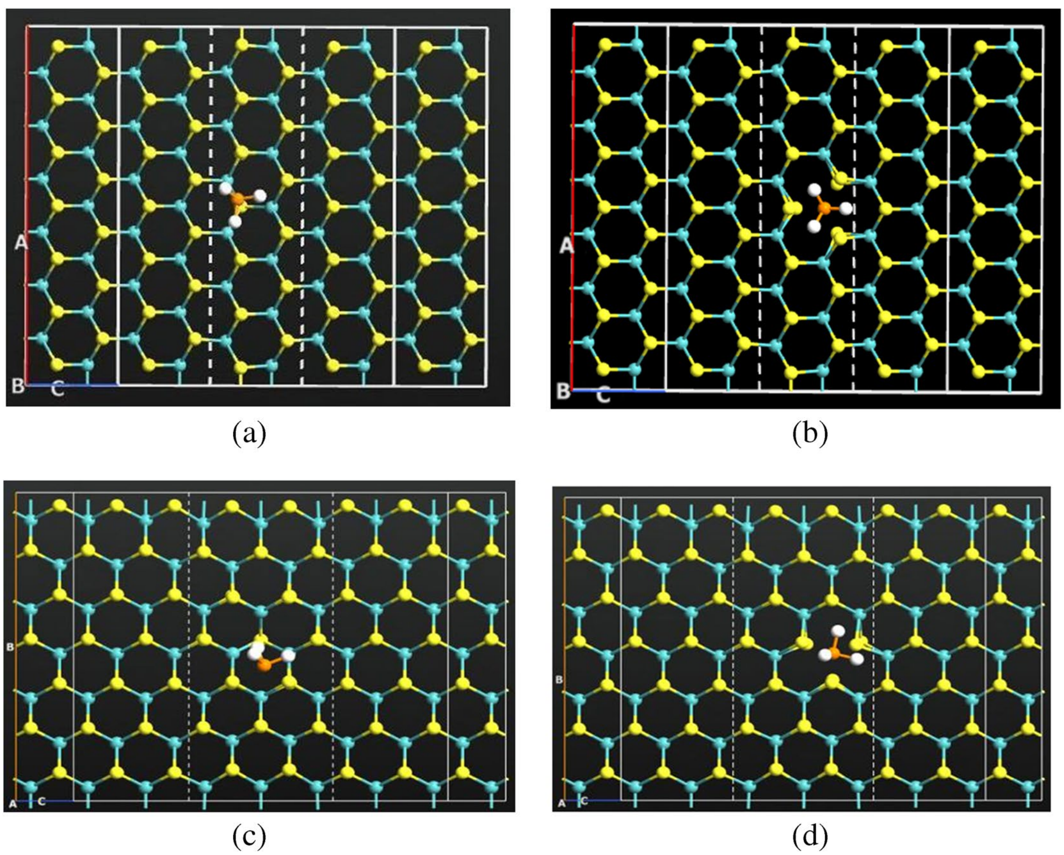

Fig. 2 Optimized structure of **a** AmS-MoS_2PH_3 device, **b** AmMo-MoS_2PH_3 device, **c** ZigS-MoS_2PH_3 device, and **d** ZigMo-MoS_2PH_3 device

for P-H_1,P-H_2, and P-H_3 (Fig. 1e), and the changes in the bond angles are 98.17°, 98.19°, and 98.32° for H_1PH_2, H_2PH_3, and H_3PH_1, respectively. Similarly, for ZigMo-MoS_2-PH_3 the changes in the bond length are 1.4503 Å, 1.5142 Å, and 1.4532 Å, and the changes in the bond angle are 93.23°, 114.30°, and 85.59°, respectively. The adsorption distance, adsorption energy, and charge transfer of the four devices are also listed in Table 1. From the Table 1, AmMo-MoS_2 and ZigMo-MoS_2 show less adsorption distance of 2.3420 Å and 2.3626 Å, more adsorption energy − 1.1048 eV and − 0.3522 eV, and more charge transfer of 0.112e and − 0.18e, respectively. From this, we observed that the PH_3 adsorption on AmMo-MoS_2 and ZigMo-MoS_2 is comparatively more.

Figure 3 shows the TDOS curve of PH_3 adsorption on AmS-MoS_2, AmMo-MoS_2, ZigS-MoS_2, and ZigMo-MoS_2. The Fermi Energy (E_F) is set to 0 eV, and this represents the zero carrier density at the Fermi region. All the four systems have not produced any changes in the bandgap after the adsorption of PH_3 gas molecule; this shows that adsorption does not introduce any mid-gap states, but near the Fermi region, some states of the AmS/Mo-MoS_2 has been changed after the PH_3 adsorption. This leads to a change in the electrical conductivity. For PH_3 adsorption on ZigS and ZigMo-MoS_2 (Fig. 3c, d), no changes are observed near the Fermi region but ZigS/Mo-MoS_2 shows a slight change (− 2.0 to − 0.5 eV) after the adsorption of PH_3 gas molecule. This indicates that the adsorption of PH_3 gas molecule considerably affects the electrical conductivity of the AmS/Mo-MoS_2 when compared with ZigS/Mo-MoS_2.

Figure 4a–d shows the projected density of states (PDOS) of AmMo-MoS_2, AmS-MoS_2, ZigS-MoS_2, and ZigMo-MoS_2 before and after the

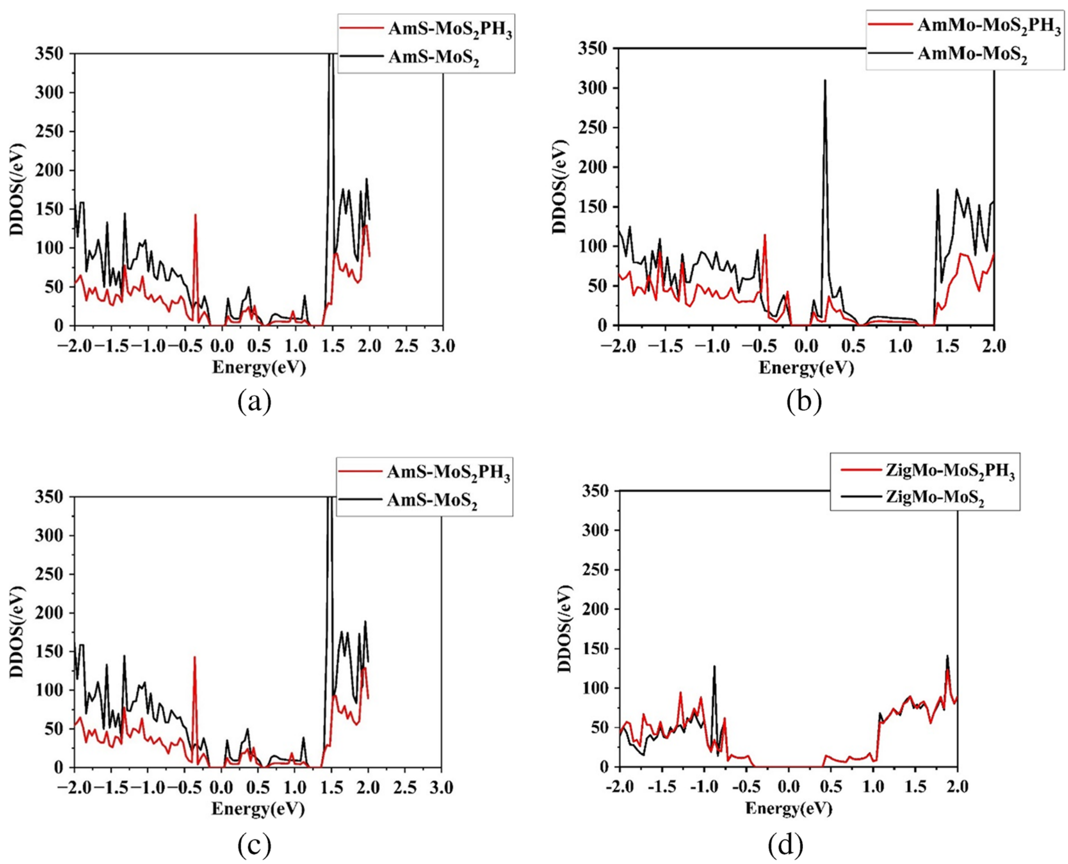

Fig. 3 TDOS of **a** AmS-MoS_2 and **b** AmMo-MoS_2 and **c** ZigS-MoS_2 and **d** ZigMo-MoS_2 before and after adsorption of PH_3 gas molecule

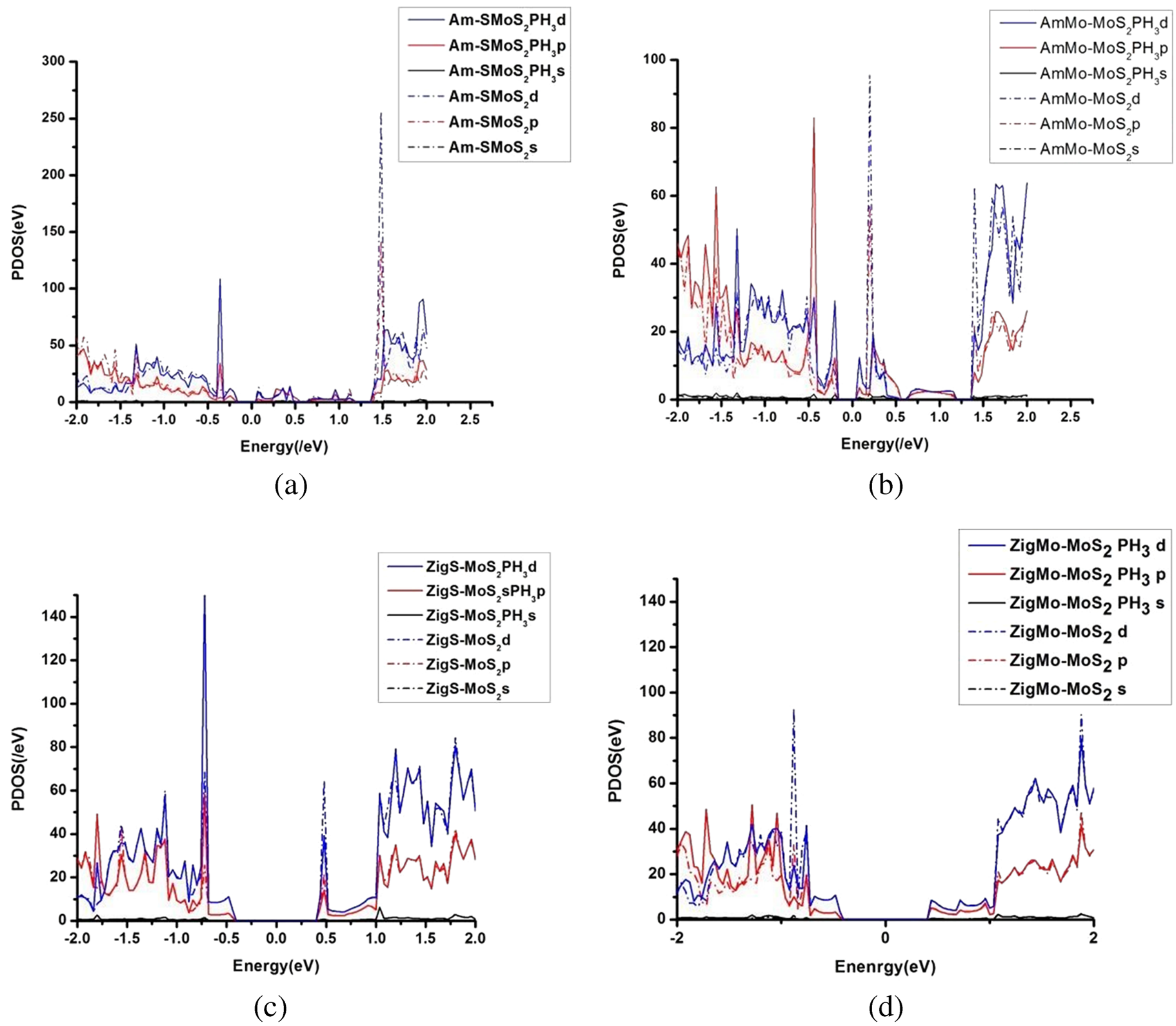

Fig. 4 PDOS of **a** AmS-MoS_2 and **b** AmMo-MoS_2 and **c** ZigS-MoS_2 and **d** ZigMo-MoS_2 before and after adsorption of PH_3 gas molecule

adsorption of PH_3 gas molecule. From Fig. 4, we observed that the PH_3 gas molecule affects the p and d orbitals of all the four systems, thus causes the changes in the TDOS after the adsorption on PH_3 gas molecule. Near the Fermi region, most of the peaks of s and d orbitals have been changed after the adsorption of PH_3 gas molecule. This indicates that there is a significant charge transfer occurred between PH_3 gas molecule and MoS_2 device and no bond formation between the gas molecule and MoS_2 device. This indicates that the changes in the peaks are caused due to van der Waals's force between the gas molecule and the system [10]. Due to these changes, the electrical conductivity of the system was changed.

The transmission spectrum of V_S and V_{MO} on the armchair and zigzag MoS_2 monolayer with and without PH_3 gas molecule are illustrated in Fig. 5a–d. From the figure, we observed that at zero bias, there is zero transmission coefficient and the width of the transmission gap are about 0.22 eV and 0.17 eV for AmS-MoS_2 and AmMo-MoS_2 and 0.82 eV and 0.81 eV for ZigS-MoS_2 and ZigMo-MoS_2, respectively, and the transmission gap acts as a barrier for electron transmission. This shows that the material has semiconducting

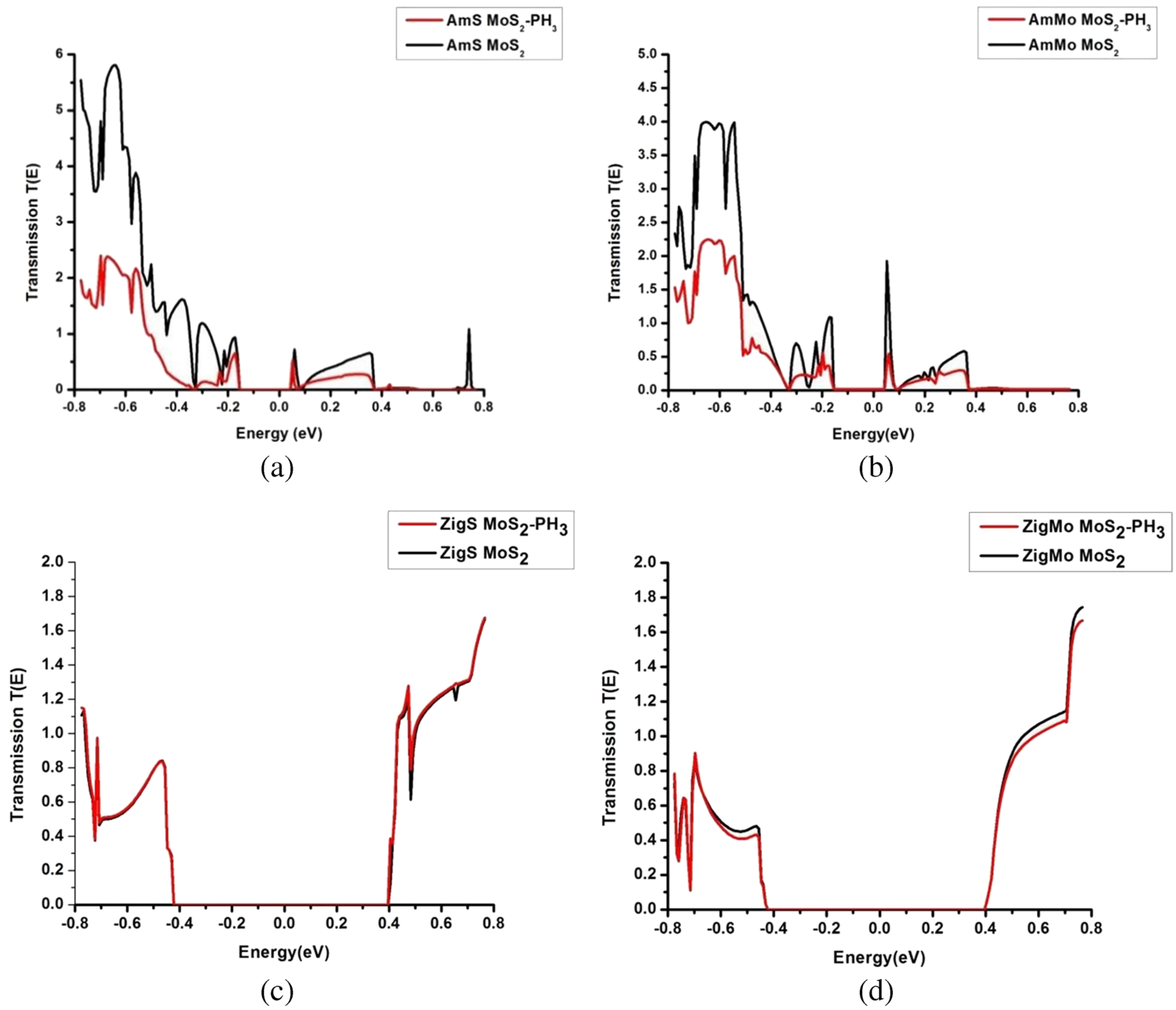

Fig. 5 Transmission spectrum of **a** AmS-MoS_2 and **b** AmMo-MoS_2 and **c** ZigS-MoS_2 and **d** ZigMo-MoS_2 before and after adsorption of PH_3 gas molecule

nature [34]. For AmS/Mo-MoS_2 (Fig. 5a, b), we observed that there is a decrease in the transmission after the adsorption of PH_3 gas molecule. The peaks in the transmission spectrum indicated the conduction channels. The reduction in the transmission peaks leads to the reduction in the current. This indicates that AmS/Mo-MoS_2 is considerably affected by the PH_3 gas molecule. For ZigS/Mo-MoS_2, the changes in the transmission are comparatively lower than AmS/Mo-MoS_2.

To clearly observe the modification in the conductivity and to qualitatively evaluate the performance of the S and Mo vacancy armchair and zigzag MoS_2 monolayer as a PH_3 sensor, the I–V characteristics of the system were analyzed, and their respective I–V graph is shown in Fig. 6. Figure 6a shows the I–V characteristics of AmS-MoS_2 with and without PH_3 adsorption. It exhibits a non-linear behavior before and after the adsorption of PH_3 gas molecule. Figure 6a shows a linear increase in the current for the bias voltage of about 0.6 to 1.2 V; the increase in the current (I_{peak}) reaches a maximum value of 0.1497 mA before the adsorption of PH_3 and 0.1192 mA after the adsorption of PH_3. This shows that the I_{peak} decreases after the adsorption of the PH_3 gas molecule.

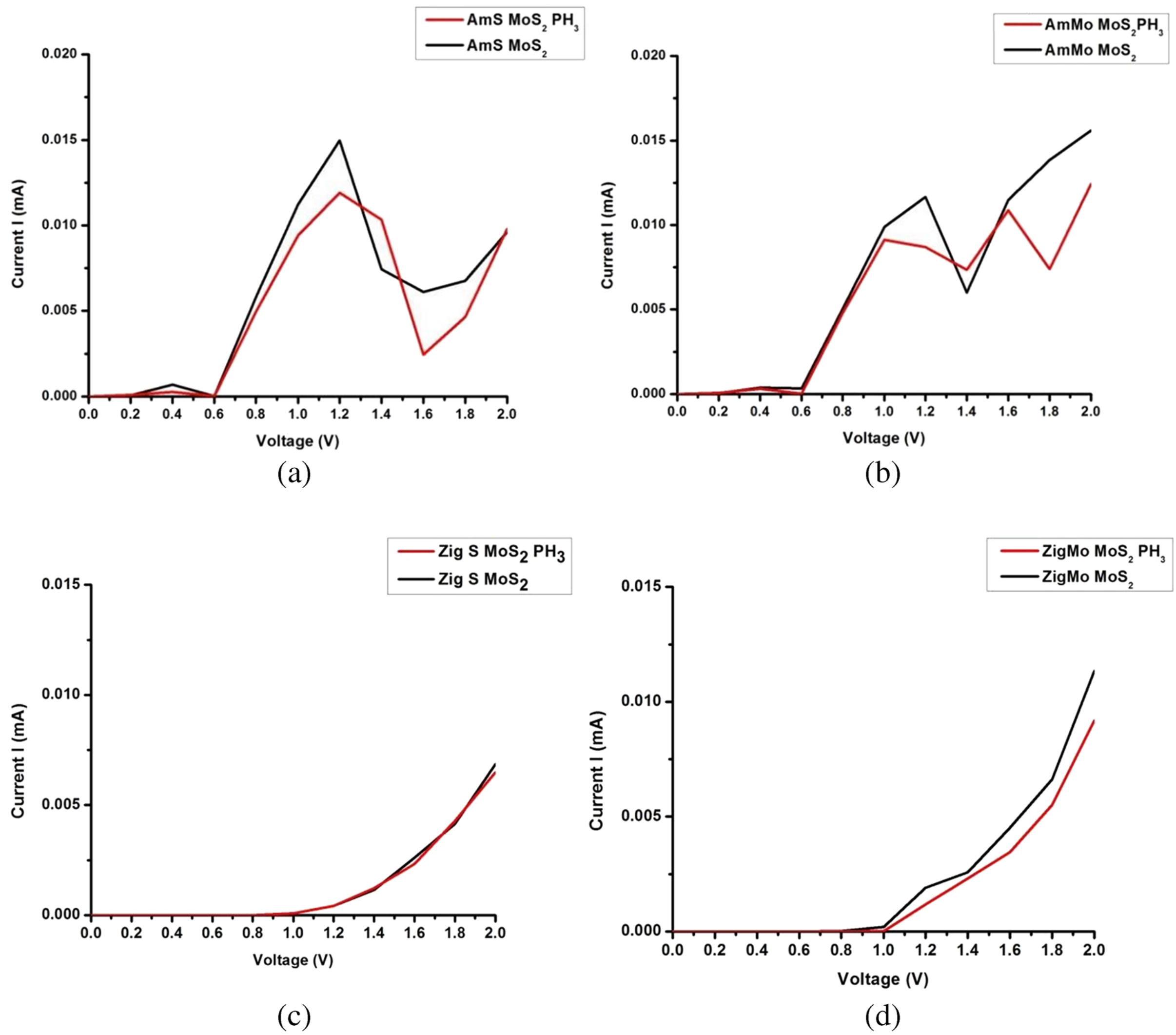

Fig. 6 I–V characteristics of **a** AmS-MoS_2 and **b** AmMo-MoS_2 and **c** ZigS-MoS_2 and **d** ZigMo-MoS_2 before and after adsorption of PH_3 gas molecule

Beyond the bias voltage of 1.2 to 1.6 V, there is a rapid decrease in the current, and the non-differential resistance (NDR) phenomena were observed [35, 36]. The decrease in the current (I_{vally}) reaches the minimum current value of 0.7345 mA before and 0.2450 mA after the adsorption of PH_3 gas molecule. This shows that there is a change in the conductivity of the material after the adsorption of PH_3 gas molecule. For PH_3, adsorption on AmMo-MoS_2 shows an increase in the current for the bias voltage of about 0.6 to 1.2 V before adsorption and 0.6 to 1.0 V after the adsorption. Here, the I_{valley} starts from 1.2 V for AmMo-MoS_2 and 1.0 V for AmMo-MoS_2PH_3; after 1.0 V, there is a reduction in current for AmMo-MoS_2 PH_3 compared with AmMo-MoS_2. The current reduction indicated the increase in the resistance of the AmS/Mo-MoS_2 PH_3 material after the adsorption of PH_3 gas molecule.

Figure 6c, d represents the I–V characteristic of PH_3 adsorption on ZigS/Mo-MoS_2 monolayer. The magnitude of the current along the ZigS/Mo-MoS_2 is smaller than AmS/Mo-MoS_2. For PH_3 adsorption on ZigS-MoS_2, there is no significant changes in the current between before and after the adsorption of PH_3 gas molecule. This shows that PH_3 gas

Table 2 The values of percentage of sensitivity of PH_3 gas molecule on AmS-MoS$_2$, AmMo-MoS$_2$, ZigS-MoS$_2$, and ZigMo-MoS$_2$ device under voltage from 0 to 2.0 V

Bias voltage/model	Percentage of sensitivity			
	AmS-MoS$_2$	AmMo-MoS$_2$	ZigS-MoS$_2$	ZigMo-MoS$_2$
0.2 V	10.45	16.78	10.78	11.32
0.4 V	32.76	35.70	12.67	12.43
0.6 V	12.67	15.87	13.98	12.99
0.8 V	25.78	14.78	15.89	17.68
1.0 V	50.65	30.67	17.84	20.67
1.2 V	50.85	88.79	19.78	70.69
1.4 V	77.98	34.98	20.65	35.89
1.6 V	70.57	40.87	23.98	60.45
1.8 V	62.87	96.87	24.67	50.65
2.0 V	13.85	86.65	24.99	72.75

molecule does not causes any change in the conductivity of the material. For PH_3 adsorption on ZigMo-MoS$_2$, the current flow is zero until the bias voltage is 0.9 V before the absorption of PH_3 and 1.0 V after the adsorption of PH_3 gas molecule. After this, the current starts increasing dramatically. Under the bias voltage of 2.0 V, the current flow through the material is 0.017 mA before and 0.014 mA after the adsorption of PH_3 gas molecule. This shows that the adsorption of PH_3 gas molecule is slightly more in ZigMo-MoS$_2$ when compared with the ZigS-MoS$_2$. The conductance for the armchair S/Mo vacancy MoS$_2$ monolayer is non-linear. The changes in the conductance before and absence of PH_3 gas molecule attribute to the response of the sensor. Therefore, for estimating the sensor response, the selectivity of the sensor is calculated using the following:

$$S = \left|G - G_0\right| / G_0 \tag{4}$$

where G and G_0 represent the conductance of Am/ZigS/Mo-MoS$_2$ after and before the gas adsorption of PH_3 gas molecule, respectively [27].

The estimated percentage of sensitivity values of the system after the adsorption of PH_3 gas molecule is listed in Table 2. Here, all the system shows different sensitivity at different bias voltage. From Table 2, we observed that the PH_3 adsorption on AmMo-MoS$_2$ shows more adsorption energy, charge transfer, and percentage of sensitivity of − 1.8048 eV, − 0.2120e, and 96.87% under the bias voltage of 1.8 V when compared with AmS-MoS$_2$, ZigS-MoS$_2$, and ZigMo-MoS$_2$ [13].

Conclusion

In this study, we have investigated the sensing behavior and electron transport property of S/Mo vacancy armchair and zigzag MoS$_2$ monolayer using NEGF-DFT techniques. The result shows that the PH_3 gas molecule is allowed to be adsorbed in all the four systems through van der Waals interaction. The structural optimization results indicate that the changes in the bond length, bond angle, and the value of the adsorption energy and charge transfer of PH_3 adsorption on AmMo-MoS$_2$ are more when compared with AmS-MoS$_2$, ZigS-MoS$_2$, and ZigMo-MoS$_2$. PH_3 adsorption on AmMo-MoS$_2$ shows better adsorption. Moreover, the changes in the PDOS and transmission spectrum are comparatively more in AmS/Mo-MoS$_2$ which leads to more changes in the I–V curve of AmS/Mo MoS$_2$, and ZigMo-MoS$_2$ indicated that there will be a change in the conductivity of the material after the adsorption of PH_3 gas molecule. Moreover, the NDR behavior was observed in both AmMo/S-MoS$_2$. AmMo-MoS$_2$ shows more changes in the current at I_{vally} after the adsorption of PH_3 gas molecule. Thus, we concluded that AmMo-MoS$_2$ shows better adsorption towards PH_3 gas molecule when compared with the other devices.

Funding We gratefully acknowledge financial support for this project from DST-FIST, Government of India (Ref. No SR/FST/PSI-155/2010).

Data availability The raw/processed data required to reproduce these findings cannot be shared at this time due to technical or time limitations.

Compliance with ethical standards

Conflict of interest The authors declare no competing interests.

References

1. Saini K, Kaushik RD (2021) Phosphine: risk assessment, environmental, and health hazard. In: Hazardous gases.

Elsevier, pp. 327–340, https://doi.org/10.1016/B978-0-323-89857-7.00012-8
2. Habibi-Yangjeh A, Basharnavaz H, Kamali SH, Nematollahzadeh A (2021) A first-principles investigation of PH3 gas adsorption on the graphitic carbon nitride sheets modified with V/P, Nb/P, and Ta/P elements. Mater Chem Phys 269:124282. https://doi.org/10.1016/j.matchemphys.2021.124282
3. Lyubimov AV, Garry VF (2010) Phosphine. In: Hayes' handbook of pesticide toxicology. Elsevier, Hardback, pp. 2259–2266
4. Pepelko B, Seckar J, Harp PR et al (2004) Worker exposure standard for phosphine gas. Risk Anal 24:1201–1213. https://doi.org/10.1111/j.0272-4332.2004.00519.x
5. Berdiyorov GR, Milošević MV, Peeters FM, van Duin ACT (2014) Stability of CH3 molecules trapped on hydrogenated sites of graphene. Phys B Condens Matter 455:60–65. https://doi.org/10.1016/j.physb.2014.07.046
6. An Y, Zhang M, Da H et al (2016) Width and defect effects on the electronic transport of zigzag MoS 2 nanoribbons. J Phys D Appl Phys 49:245304. https://doi.org/10.1088/0022-3727/49/24/245304
7. Feng C, Qin H, Yang D, Zhang G (2019) First-principles investigation of the adsorption behaviors of CH2O on BN, AlN, GaN, InN, BP, and P monolayers. Materials (Basel) 12:676. https://doi.org/10.3390/ma12040676
8. Cheng M, Chen Q, Yang K et al (2019) Penta-graphene as a potential gas sensor for NOx detection. Nanoscale Res Lett 14:306. https://doi.org/10.1186/s11671-019-3142-4
9. Zhou Y, Dong J, Li H (2015) Electronic transport properties of in-plane heterostructures constructed by MoS 2 and WS 2 nanoribbons. RSC Adv 5:66852–66860. https://doi.org/10.1039/C5RA14507D
10. Jasmine JM, Aadhityan A, Preferencial Kala C, Thiruvadigal DJ (2019) A first-principles study of Cl2, PH3, AsH3, BBr 3 and SF4 gas adsorption on MoS2 monolayer with S and Mo vacancy. Appl Surf Sci 489:841–848. https://doi.org/10.1016/j.apsusc.2019.05.197
11 Barzegar M, Berahman M, IrajiZad A (2018) Sensing behavior of flower-shaped MoS 2 nanoflakes: case study with methanol and xylene. Beilstein J Nanotechnol 9:608–615. https://doi.org/10.3762/bjnano.9.57
12. Zhang J, Yang G, Tian J et al (2018) First-principles study on the gas sensing property of the Ge, As, and Br doped PtSe 2. Mater Res Express 5:035037. https://doi.org/10.1088/2053-1591/aab4e3
13. Srivastava M, Srivastava A (2019) Electron transport in CO2 adsorbed ZnO nanowire: DFT study. Chem Phys Lett 729:17–23. https://doi.org/10.1016/j.cplett.2019.05.014
14. Jin W, Guofeng Y, Junjun X et al (2018) High sensitivity and selectivity of AsP sensor in detecting SF6 decomposition gases. Sci Rep 8:12011. https://doi.org/10.1038/s41598-018-30643-y
15. Perkins FK, Friedman AL, Cobas E et al (2013) Chemical vapor sensing with monolayer MoS2. Nano Lett 13:668–673. https://doi.org/10.1021/nl3043079
16. Kou L, Frauenheim T, Chen C (2014) Phosphorene as a superior gas sensor: selective adsorption and distinct I – V response. J Phys Chem Lett 5:2675–2681. https://doi.org/10.1021/jz501188k
17. Novoselov KS, Jiang D, Schedin F et al (2005) Two-dimensional atomic crystals. Proc Natl Acad Sci 102:10451–10453. https://doi.org/10.1073/pnas.0502848102
18. Coleman JN, Lotya M, O'Neill A et al (2011) Two-dimensional nanosheets produced by liquid exfoliation of layered materials. Science 331:568–571. https://doi.org/10.1126/science.1194975
19. Shokri A, Salami N (2016) Gas sensor based on MoS2 monolayer. Sensors Actuators B Chem 236:378–385. https://doi.org/10.1016/j.snb.2016.06.033
20. Ren J, Liu H, Xue Y, Wang L (2019) Adsorption behavior of CH4 gas molecule on the MoX2(S, Se, Te) monolayer: the DFT study. Nanoscale Res Lett 14:293. https://doi.org/10.1186/s11671-019-3125-5
21. Feng L, Su J, Liu Z (2014) Effect of vacancies on structural, electronic and optical properties of monolayer MoS2: a first-principles study. J Alloys Compd 613:122–127. https://doi.org/10.1016/j.jallcom.2014.06.018
22. Zhao S, Xue J, Kang W (2014) Gas adsorption on MoS2 monolayer from first-principles calculations. Chem Phys Lett 595–596:35–42. https://doi.org/10.1016/j.cplett.2014.01.043
23. Wei H, Gui Y, Kang J et al (2018) A DFT study on the adsorption of H2S and SO2 on Ni doped MoS2 monolayer. Nanomaterials 8:646. https://doi.org/10.3390/nano8090646
24. Kumar R, Zheng W, Liu X et al (2020) MoS2 -based nanomaterials for room-temperature gas sensors. Adv Mater Technol 5:1901062. https://doi.org/10.1002/admt.201901062
25. Chacko L, Massera E, Aneesh PM (2020) Enhancement in the selectivity and sensitivity of Ni and Pd functionalized MoS 2 toxic gas sensors. J Electrochem Soc 167:106506. https://doi.org/10.1149/1945-7111/ab992c
26. Dandeliya S, Srivastava A (2015) Carbon nanotube based NH_3 gas sensor: ab-initio study. In: 2015 IEEE Intern Symp Nanoelectronic Inform Sys. IEEE, pp. 268–271. https://doi.org/10.1109/iNIS.2015.54
27. Meribah Jasmine J, Preferencial Kala C, John Thiruvadigal D (2021) First principle study of adsorption behavior of PF5 gas molecule on S and Mo vacancy MoS2 monolayer. J Electron Mater 50:1668–1677. https://doi.org/10.1007/s11664-020-08480-5
28. Torres I, Mehdi Aghaei S, RabieiBaboukani A et al (2018) Individual gas molecules detection using zinc oxide–graphene hybrid nanosensor: a DFT study. C 4:44. https://doi.org/10.3390/c4030044
29. Janani K, John Thiruvadigal D (2018) Adsorption of essential minerals on l-glutamine functionalized zigzag graphene nanoribbon-a first principles DFT study. Appl Surf Sci 449:829–837. https://doi.org/10.1016/j.apsusc.2018.02.137
30. Zhong H, Quhe R, Wang Y et al (2016) Interfacial properties of monolayer and bilayer MoS2 contacts with metals: beyond the energy band calculations. Sci Rep 6:21786. https://doi.org/10.1038/srep21786
31. Saha D, Mahapatra S (2016) Theoretical insights on the electro-thermal transport properties of monolayer MoS 2 with line defects. J Appl Phys 119:134304. https://doi.org/10.1063/1.4945582

32. Zhao Z, Yong Y, Zhou Q et al (2020) Gas-sensing properties of the SiC monolayer and bilayer: a density functional theory study. ACS Omega 5:12364–12373. https://doi.org/10.1021/acsomega.0c01084
33. Shahab S, Sheikhi M, Khaleghian M et al (2018) DFT study of physisorption effect of CO and CO2 on furanocoumarins for air purification. J Environ Chem Eng 6:4784–4796. https://doi.org/10.1016/j.jece.2018.07.019
34. Cao J, Logoteta D, Ozkaya S et al (2016) Operation and design of van der Waals tunnel transistors: a 3-D quantum transport study. IEEE Trans Electron Devices 63:4388–4394. https://doi.org/10.1109/TED.2016.2605144
35. Kaewmaraya T, Ngamwongwan L, Moontragoon P et al (2021) Novel green phosphorene as a superior chemical gas sensing material. J Hazard Mater 401:123340. https://doi.org/10.1016/j.jhazmat.2020.123340
36. Cheng Y, Meng R, Tan C et al (2018) Selective gas adsorption and I-V response of monolayer boron phosphide introduced by dopants: a first-principle study. Appl Surf Sci 427:176–188. https://doi.org/10.1016/j.apsusc.2017.08.187